AIAA JOURNAL
Vol. 46, No. 4, April 2008

Simulation and Parameter Variation of Flapping-Wing Motion Based on Dragonfly Hovering

John Young* and Joseph C. S. Lai†
University of New South Wales,
Australian Defence Force Academy, Canberra, Australian Capital Territory 2600, Australia
and
Charly Germain‡
Institut National des Sciences Appliquées de Lyon, 69100 Villeurbanne, France

DOI: 10.2514/1.31610

The flapping motion of a wing based on the hind wing of the *Aeschna juncea* dragonfly is simulated using a three-dimensional incompressible Navier–Stokes solver. The performance of the wing is investigated by variation of a number of kinematic parameters. Flapping amplitudes of between 10 and 60 deg (half-angle) and frequencies of 1 to 300 Hz are considered, resulting in a Reynolds number range of 100 to 50,000. The flapping amplitude observed for *Aeschna juncea* is shown to maximize the ratio of mean vertical force produced to power required.

Nomenclature

b	=	wing span
$\bar{C}_H$, $\bar{C}_V$	=	time-averaged horizontal and vertical force coefficients
$\bar{C}_P$	=	time-averaged power coefficient
c	=	mean aerodynamic chord
$\bar{F}_H$, $\bar{F}_V$	=	time-averaged horizontal and vertical aerodynamic forces
f	=	flapping frequency, Hz
$\bar{P}$	=	time-averaged aerodynamic power required
Re	=	Reynolds number, $V_W c/\nu$
S	=	wing area
T	=	f^{-1}, flapping period, s
V_i	=	velocity of the air induced by the wing motion
V_W	=	maximum translational velocity of the wing (at 2/3 span)
α_D, α_U	=	wing angle of attack during downstroke and upstroke
$\Delta\tau_R$	=	duration of wing rotation, as a fraction of the period
ν	=	kinematic viscosity
τ	=	t/T, nondimensional time (fraction of the flapping stroke, starting from the beginning of the downstroke)
τ_D, τ_U	=	start of wing rotation on the downstroke and upstroke, as a fraction of the period
ϕ_0	=	flapping amplitude (centerline to peak) such that $\phi(t) = \phi_0 \cos(2\pi f t)$

Presented as Paper 2006-38 at the 44th Aerospace Sciences Meeting and Exhibit, Reno, NV, 9–12 January 2006; received 15 April 2007; accepted for publication 13 November 2007.

*Lecturer, School of Aerospace, Civil and Mechanical Engineering; j.young@adfa.edu.au. Member AIAA.
†Professor, School of Aerospace, Civil and Mechanical Engineering. Associate Fellow AIAA.
‡Exchange Student, School of Aerospace, Civil and Mechanical Engineering. UNSW@ADFA.

I. Introduction

FLIGHT in nature has long served as the inspiration for human-designed flying vehicles. As designers strive to create smaller micro air vehicles (MAVs) for such tasks as urban reconnaissance and search-and-rescue missions, various biological flight mechanisms have been considered (see, for example, Ellington [1] and Mueller [2]). Among these, the ability to hover (and land and take off vertically) is a very useful trait for such vehicles, and thus it is natural to examine the aerodynamics of animals such as birds and insects that are capable of hovering.

In a recent review article, Wang [3] cited Weis-Fogh [4] as distinguishing two overall categories of wing motion in hovering insects. In so-called normal hovering, used by a majority of insects, the wings undergo symmetric motion in an approximately horizontal stroke plane. In inclined-stroke-plane hovering, used by dragonflies and hoverflies, the angle of attack and the force generated are greater during the downstroke, and the stroke plane is significantly inclined from the horizontal. There is a wide body of literature, including both experimental and computational studies, examining various hovering insects with relatively small stroke-plane inclinations. For example, Dickinson et al. [5] and Dickinson [6] discussed various elements of lift production by delayed stall (highlighting the importance of leading-edge-vortex formation), rotational lift, and wake-capture mechanisms for a fruit fly; Altshuler et al. [7] explored the relative importance of flapping frequency and amplitude for lift generation by a honeybee; Liu et al. [8] examined the role of the leading-edge vortex on a hawkmoth wing; Sane and Dickinson [9] determined the effect of wing angle of attack, rotation timing, and wing deviations from the stroke plane on lift production for a fruit fly wing.

Dragonflies have also been the subject of considerable analysis (for example, Norberg [10] and Wakeling and Ellington [11]), although the aerodynamic mechanisms are less clear. Wang [12] showed via 2D computation that dragonfly-style hovering with a large stroke-plane inclination (approximately 60 deg) relies substantially on drag to generate vertical force and also that this mode of hovering may require less power than a symmetrical horizontal stroke for the same vertical force. Sun and Lan [13] used a 3D computational solver to estimate the vertical force production and power requirements for a dragonfly in one flight condition and showed vertical force being created by downward-moving vortex rings. Yamamoto and Isogai [14] studied the effect of phase angle between fore and hind wings via experiment and 3D computation. In the present work, a Navier–Stokes computational solver is used to study the performance of flapping-wing motions based on the dragonfly hovering mode. The object is not to simulate the precise

kinematics and aerodynamics of a particular insect, but rather to determine performance trends with variation of fundamental flapping parameters such as the amplitude, frequency, and rotation timings.

II. Computational Procedure and Validation

A. Wing Kinematics

To minimize the number of parameters to be varied, only a single wing is considered. The wing is based on the hind wing of the *Aeschna juncea* dragonfly, as shown in Fig. 1, approximating that used by Sun and Lan [13] and derived from Norberg [15]. Sun and Lan [13] and Yamamoto and Isogai [14] noted that the interaction between the fore and hind wings, and the subsequent effect on forces generated by the wings when considered singly, is minimal. This was clarified by Huang and Sun [16], who showed that the interaction is minimal for motions in which the hind wing leads the forewing.

The wing is modeled as a rigid flat plate with span $b = 4.6$ cm, mean aerodynamic chord $c = 1.22$ cm, and thickness equal to 1% of c. The pivot point of the wing is placed on the wing root, at a distance $c/4$ aft of the leading edge. The wing undergoes flapping $\phi(t) = \phi_0 \cos(2\pi f t)$ along the stroke plane (wingtip upward positive) and pitching rotation $\theta(t)$ about an axis which moves with the wing, as shown in Fig. 2. The rotation of the wing is modeled as per Sun and Lan [13] with periods of constant angle of attack on the downstroke and upstroke and rotations (leading-edge upward positive) starting at τ_D on the downstroke, τ_U on the upstroke, and each of duration $\Delta\tau_R$ (equations repeated here for completeness):

$$\dot{\theta}(\tau) = 0.5\dot{\theta}_0\{1 - \cos(2\pi[\tau - \tau_D]/\Delta\tau_R)\}$$
$$\text{for } \tau_D < \tau < \tau_D + \Delta\tau_R \qquad (1)$$
$$\dot{\theta}_0 = (\pi - \alpha_U - \alpha_D)/(\Delta\tau_R T)$$

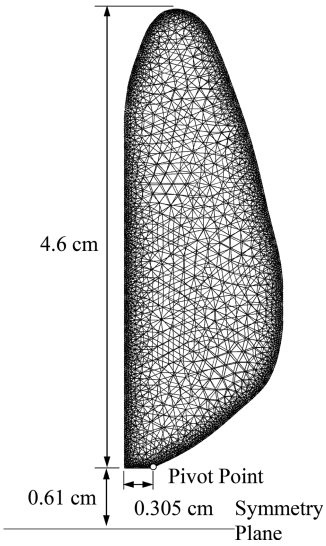

Fig. 1 Wing planform based on hind wing of dragonfly *Aeschna juncea*.

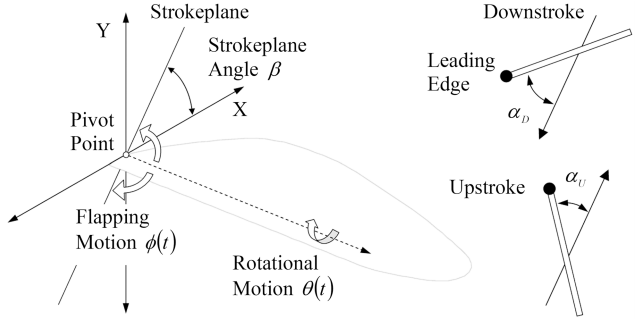

Fig. 2 Wing kinematics.

with $\theta(\tau) = \alpha_D$ at $\tau = \tau_D$ and $\theta(\tau) = \pi - \alpha_U$ at $\tau = \tau_D + \Delta\tau_R$ for the rotation at the bottom of the downstroke. The rotation at the top of the upstroke is calculated similarly, with the sign of $\dot{\theta}_0$ reversed and τ_U substituted for τ_D.

A symmetry plane is imposed aligned with the X–Y plane (along the centerline of the dragonfly, although the body is not modeled here). The pivot point is set at the wing root (rather than the symmetry plane as in Sun and Lan [13]) to enable a large range of flapping amplitudes to be considered without the wing colliding with its reflection. This is compatible with the object of determining performance trends rather than simulating one insect exactly.

The reference velocity for nondimensionalization is calculated as the maximum translational velocity of the wing at an arbitrarily chosen distance of 2/3 of the span out from the pivot point, $V_W = (4\pi/3)b\phi_0 f$. The Reynolds number based on chord is

$$Re = \frac{V_W c}{\nu} = \frac{4\pi}{3}\frac{b}{c}\phi_0\frac{fc^2}{\nu} \qquad (2)$$

The Reynolds number is seen to be a product of three nondimensional elements: the aspect ratio b/c, flapping amplitude ϕ_0, and a nondimensional frequency $\hat{f} = fc^2/\nu$. This replaces the usual reduced frequency $k = fc/V_W$, which reduces to a purely geometric parameter for hovering flight. The Reynolds numbers considered in the present work range from approximately 100 to 50,000.

The power required to move the wing against the aerodynamic forces is calculated as

$$P = -(M_X\dot{\gamma}_X + M_Y\dot{\gamma}_X + M_Z\dot{\gamma}_Z)$$

where M_X, M_Y, and M_Z are the aerodynamic moments about the pivot point, measured in inertial XYZ coordinates, and $\dot{\gamma}_X$, $\dot{\gamma}_Y$, and $\dot{\gamma}_Z$ are the instantaneous rotation rates of the wing about those axes. Mean force coefficients $\bar{C}_V$ and $\bar{C}_H$, measured in the Y and X inertial directions, respectively, and the mean power coefficient $\bar{C}_P$ are averaged over one flapping cycle:

$$\bar{C}_V = \frac{2}{\rho V_W^2 S}\frac{1}{T}\int_t^{t+T} F_V\,\mathrm{d}t, \qquad \bar{C}_H = \frac{2}{\rho V_W^2 S}\frac{1}{T}\int_t^{t+T} F_H\,\mathrm{d}t$$
$$\bar{C}_P = \frac{2}{\rho V_W^3 S}\frac{1}{T}\int_t^{t+T} P\,\mathrm{d}t \qquad (3)$$

The motion of the insect body (and thus of the wing pivot point) in response to a nonconstant vertical force has been ignored in the present work. As discussed by Sun and Lan [13], the combined force generated by the dragonfly fore and hind wings varies at approximately twice the flapping frequency, because the wing pairs beat somewhat out of phase. For the sake of estimating the magnitude of the body motion, the total vertical force can be simply modeled as a sinusoid with a time-averaged value equal to the weight of the insect: $F(t) = mg(1 + \sin(4\pi f t))$. Ignoring any damping effect due to aerodynamic drag on the insect body, the body motion is thus modeled as

$$m\ddot{y}(t) = F(t) - mg = mg\sin(4\pi f t)$$

resulting in a magnitude $|y| = g/(4\pi f)^2$. For a flapping frequency $f = 30$ Hz, at which the majority of simulations were performed, this gives a magnitude of body motion due to nonconstant vertical force of approximately 0.07 mm and a body velocity of 0.026 m/s (compared with fluid flow velocities exceeding 12 m/s in the simulations), both of which are negligible on the scale of these simulations and can be ignored. For frequencies below 5 Hz, the results presented will not represent a true hover situation, in that the body motion would be significant and would require a more detailed analysis involving both wing pairs and the body as well as fluid–structure interaction. Nevertheless, the calculations presented here will be able to illustrate the performance trend (in particular, in the frequency range 5–300 Hz) due to the influence of fundamental flapping parameters.

B. Computational Solver and Grid

The unsteady incompressible Navier–Stokes equations are solved using the commercial software package Fluent 6.2. The wing motion is incorporated via the dynamic mesh feature using a user-defined function to describe the kinematics. Second-order spatial discretizations are used, and the pressure-velocity coupling is via the semi-implicit method for pressure-linked equations (SIMPLE) algorithm. Note that Fluent is currently limited to first-order time stepping when the dynamic mesh feature is used. Residuals are reduced by two orders of magnitude at each time step.

The grid, shown partially in Fig. 3, is constructed in two parts. The wing is surrounded by a layer of cells that moves as a rigid body with the wing. This inner region is enclosed in a stationary outer region in which the cells are deformed or remeshed at each time step, to accommodate the motion of the wing and inner region. The boundary of the outer region is hemispherical, at a distance of approximately 10 wingspans from the origin.

Cells are clustered on the wing surface near the edges of the wing and within the inner region. In this way, as the wing and inner region move, a boundary layer of small cells is maintained around the wing. Although cells toward the center of the wing are quite large in comparison with those around the edges, the sharp-edged nature of the flat-plate model ensures that flow separation occurs at the wing edges, and thus details of the boundary-layer flow are less important in the wing center. This is discussed further in Sec. II.C.

C. Verification and Validation

Two grids and a number of time steps per flapping cycle were tested for the case of $\phi_0 = 34.5$ deg and $f = 30.0$ Hz ($Re = 2950$). The first grid (163,000 grid) consisted of 162,507 tetrahedral cells (10,854 total triangular cells on the wing surface). The second grid (890,000 grid), consisting of 890,079 tetrahedral cells (40,515 total triangular cells on the wing surface), was constructed from the 163,000 grid by halving the spatial dimension of all cells in a hemisphere surrounding the wing and inner region. All runs were calculated for four flapping cycles, at which point starting transients had disappeared and the aerodynamic forces were periodic. Figure 4 shows the variation of vertical force coefficient for the two grids with 200 steps per cycle and for the 163,000 grid with 50, 100, 200, and 400 steps per cycle. There is very little variation apparent in the vertical force coefficient, and the horizontal force, moment, and power coefficients all display the same level of similarity (not shown here). All subsequent calculations use the 163,000 grid with 200 time steps per flapping cycle, for which the force results can be considered approximately grid- and time-step-independent.

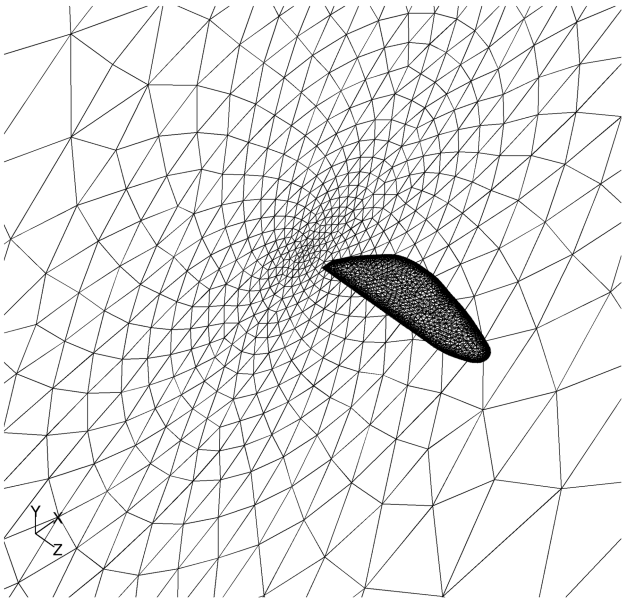

Fig. 3 Grid on the wing and symmetry plane.

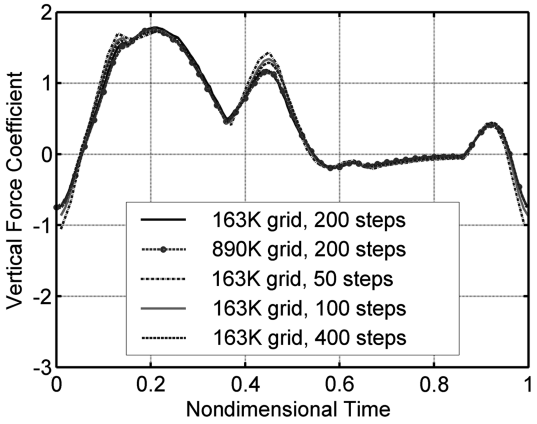

Fig. 4 Grid and time-step refinement.

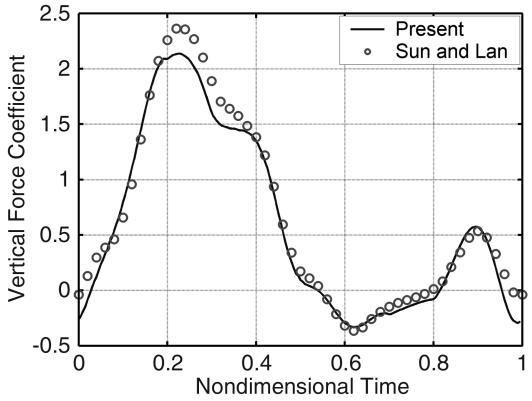

Fig. 5 Comparison with Sun and Lan [13] results.

The single hind-wing calculations of Sun and Lan [13] ($\beta = 52$ deg, $\alpha_D = 52$ deg, $\alpha_U = 8$ deg, and $f = 36$ Hz, resulting in approximately $Re = 3540$) were also repeated for comparison. The wing rotation times were not stated explicitly, and so these were estimated (via curve-fitting Fig. 5a in [13]) as $\tau_D = 0.305$, $\tau_U = 0.805$, and $\Delta\tau_R = 0.4$. The results for the vertical force coefficient are shown in Fig. 5. The present calculations agree very closely with those of Sun and Lan [13], except at the top of the upstroke and bottom of the downstroke. Given the minor differences in the wing shape (Sun and Lan [13] have a squared-off wingtip, and the mean chord is slightly different), the level of agreement is taken to be sufficiently close.

Because the wing is modeled as a sharp-edged flat plate, the separation point is effectively fixed at the wing edges for all Reynolds numbers; thus, grid and time-step validation at an intermediate Reynolds number is considered sufficient to ensure that the flow behavior is captured across the Reynolds number range considered. Two further calculations, using laminar flow and the detached-eddy-simulation turbulence model, were performed for $\phi_0 = 34.5$ deg with $f = 5.0$ Hz ($Re = 484$) and $\phi_0 = 34.5$ deg with $f = 300.0$ Hz ($Re = 29,048$) on the 163,000 grid. There were essentially no differences in aerodynamic forces between laminar and turbulent calculations in either case, again attributed to the sharp wing edges fixing the flow separation point. All further calculations performed herein assume laminar flow. Note that further investigation is required with a much more detailed wing model (in particular, a more accurate leading-edge geometry) to establish the importance of any variation in the separation point at different Reynolds number.

III. Results and Analysis

A. Amplitude and Frequency Variation

Flapping amplitude and frequency were varied to determine the sensitivity of the aerodynamic forces, moments, and power

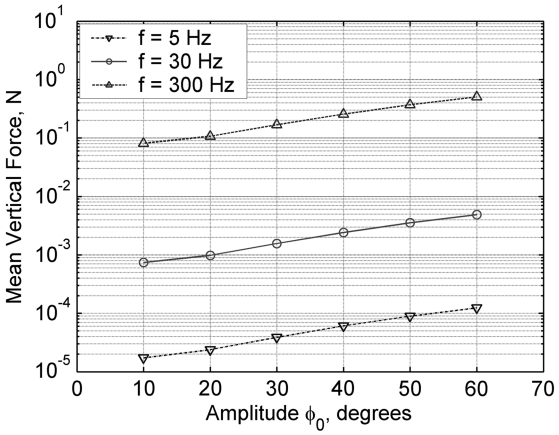

Fig. 6 Mean vertical force variation with flapping amplitude.

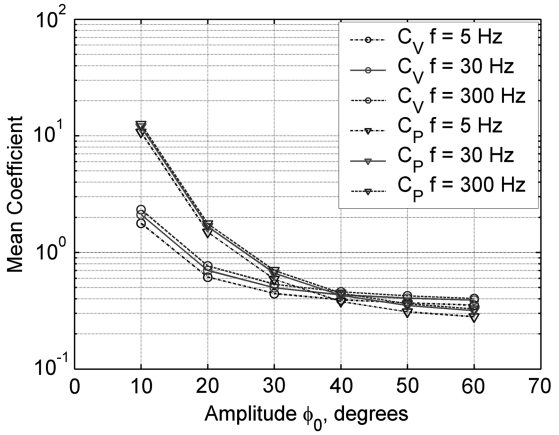

Fig. 8 Mean vertical force and power-coefficient variations with flapping amplitude.

requirements. Wing angles of attack $\alpha_D = 58$ deg and $\alpha_U = 8$ deg and rotation timings $\tau_D = 0.36$, $\tau_U = 0.86$, and $\Delta\tau_R = 0.29$ were maintained throughout. The stroke plane was set at $\beta = 60$ deg for each simulation, then recalculated by a coordinate rotation so that $\bar{C}_H = 0$ in each case (i.e., the wing is genuinely in hover). Note that the wing is flapping in initially quiescent air, and so there is no preferred reference frame for the calculations. All simulations were done at the same stroke plane for convenience, then the reference frame rotated appropriately a posteriori, and so the initial stroke-plane angle is immaterial to the final result. Figures 6 and 7 show the mean vertical force developed and mean aerodynamic power required to drive the wing, in the amplitude range $\phi_0 = 10$–60 deg and frequencies $f = 5, 10$, and 300 Hz. Both vertical force and power increase monotonically with flapping amplitude. When non-dimensionalized using the maximum wing velocity V_W, the mean vertical force and power coefficients become relatively insensitive to frequency, as shown in Fig. 8. Similar results were reported and discussed in detail for both rotating and flapping wings (e.g., Usherwood and Ellington [17] and Wu and Sun [18]).

The stroke-plane angle decreases sharply as amplitude decreases in Fig. 9, which is to be expected as the effect of rotation begins to dominate over that of translation (in the limit of no translation, the wing would just rotate between α_D and 180 deg $-\alpha_U$, with the net force in a direction halfway between these two angles). The stroke-plane angle at high amplitudes is similar to that reported in the literature for dragonflies (Wang [3], Sun and Lan [13], and Norberg [10]).

We may define a hover efficiency for the wing as the mean power induced in the air, divided by the mean power required to drive the wing:

$$\eta_H = \frac{\bar{F}_V V_i}{\bar{P}} \tag{4}$$

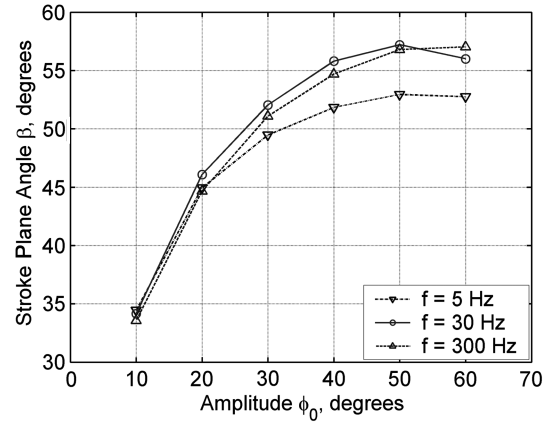

Fig. 9 Stroke-plane-angle variation with flapping amplitude.

where V_i is the air velocity induced by the wing as if it were an ideal actuator disk of equal area. This may be estimated from conservation of mass and momentum (see, for example, Vogel [19], pp. 274–275) as

$$V_i = \sqrt{\frac{\bar{F}_V}{2\rho S}} = \sqrt{\frac{\bar{C}_V(1/2)\rho V_W^2 S}{2\rho S}} = \frac{V_W}{2}\sqrt{\bar{C}_V} \tag{5}$$

Figures 10 and 11 show the hover efficiency of the wing as a function of flapping frequency and amplitude. At large enough frequencies, the efficiency plateaus and becomes primarily a function of the flapping amplitude. These figures might suggest that it would be advantageous to flap simultaneously at both the highest frequency

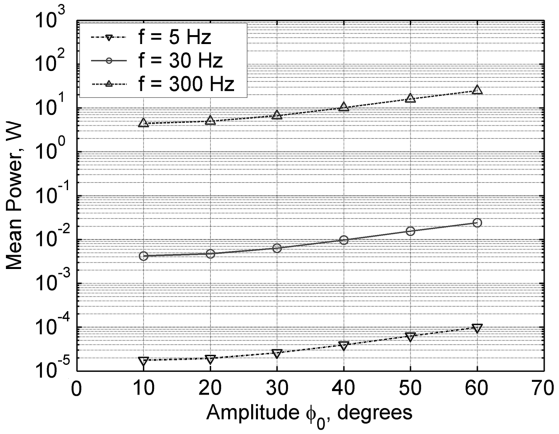

Fig. 7 Mean power variation with flapping amplitude.

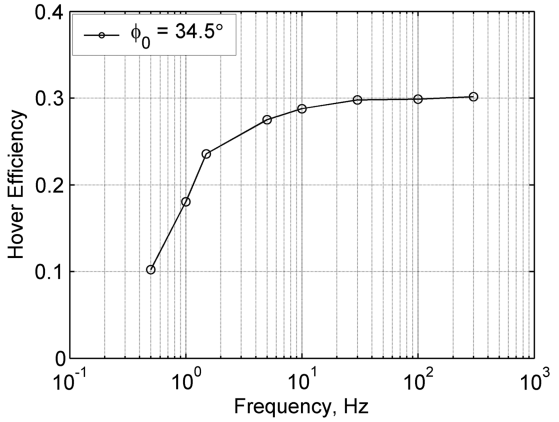

Fig. 10 Hover-efficiency variation with flapping frequency.

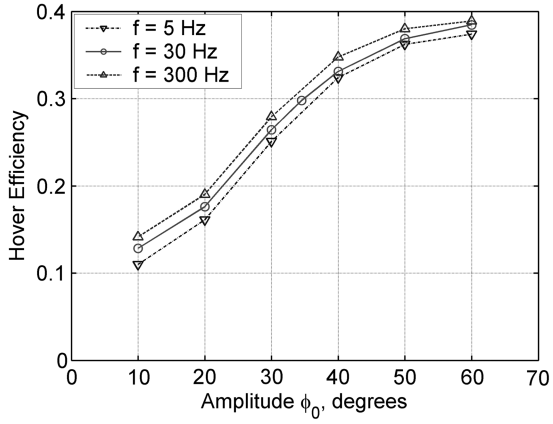

Fig. 11 Hover-efficiency variation with flapping amplitude.

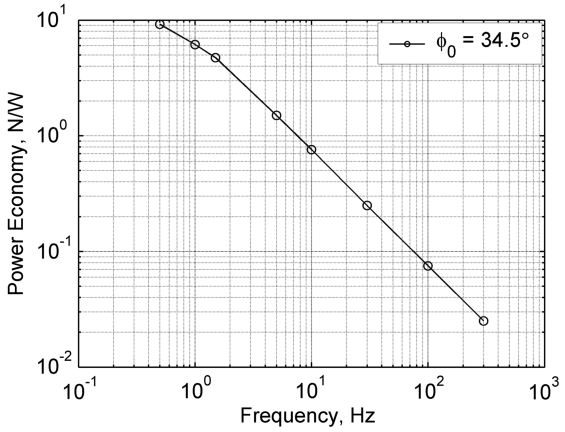

Fig. 12 Power-economy variation with flapping frequency.

and highest amplitude possible, to achieve the highest efficiency. However, this results in very high power requirements, as shown by Fig. 7.

A more useful measure of performance is obtained by examining the "power economy," a ratio of the mean vertical force produced to the mean power required:

$$\mathrm{PE} = \frac{\bar{F}_V}{\bar{P}} \tag{6}$$

which is just the hover efficiency divided by the ideal induced velocity V_i. Figures 12 and 13 show the power economy as a function of frequency and amplitude. In Fig. 13, the power economy was scaled by a factor equal to $f/30$, so that all three frequency curves may be easily viewed on the same graph.

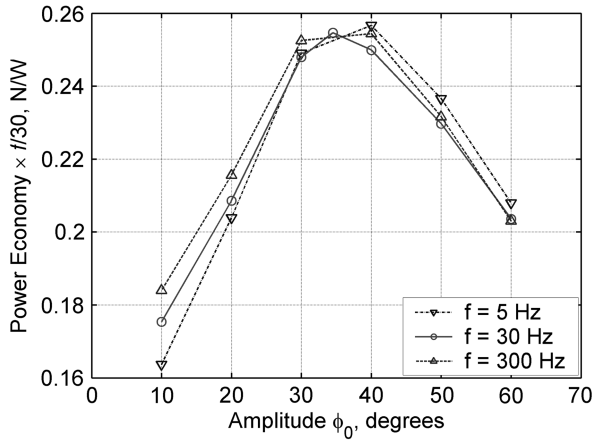

Fig. 13 Scaled power-economy variation with flapping amplitude.

Unlike the hover efficiency, which is monotonic with flapping amplitude, the power economy shows a pronounced peak at approximately $\phi_0 = 35$ deg for all the frequencies considered, which is very close to the amplitude observed for the *Aeschna juncea* dragonfly (Sun and Lan [13] and Norberg [15]). Taken together, Figs. 6 and 13 show how flapping frequency and amplitude might be set for an insect (or vehicle) employing the wing motion considered here. The required vertical force in a stationary hover is fixed by the weight, and so the power required for flapping is minimized by maximizing the power economy at approximately $\phi_0 = 35$ deg. The frequency is then varied until the required vertical force is generated.

It is interesting to note that Altshuler et al. [7], examining the flight of honeybees (which use a "normal hovering" rather than a "dragonfly hovering" wing motion), found that when challenged to fly in low-density air, the bees maintained flapping frequency and increased amplitude, whereas the preceding results would imply maintaining amplitude at an optimum value. Further work is required to determine the sensitivity of the results shown in Fig. 13 to changes in wing geometry and kinematics: in particular, whether they hold for normal hovering as well as dragonfly hovering. Also, wing flexibility in response to aerodynamic loading should be investigated for its effect on the power economy.

Figure 14 shows instantaneous streamlines for a range of flapping amplitudes at $f = 30$ Hz as the wing moves downward past the horizontal (nondimensional time $t/T = 0.6$). A spiral vortex forms over the leading edge of the wing, increasing in strength with increasing flapping amplitude. For lower amplitudes, the vortex remains attached over the entire span of the wing; however, at higher amplitudes, the vortex bursts over the outboard section of the wing. Animations of the vorticity field show consistent features up to $\phi_0 = 34.5$ deg, with a vortex ring directed backward by the wing rotation at the top of the upstroke and a second vortex ring responsible for the majority of the vertical force, created by the downstroke. At amplitudes of $\phi_0 = 40$ deg and greater, the wing passes through this second vortex ring on the upstroke and part of the vortex ring is then redirected to create a forward, rather than vertical, force. In this manner, separation of the leading-edge vortex may be responsible for the reduction in power economy as amplitude is increased beyond $\phi_0 = 34.5$ deg.

B. Wing Rotation Variation

The rate at which the wing is rotated at the extremes of the flapping stroke was varied to separate and examine performance effects due to translational and rotational velocities. As a baseline, Figs. 15 and 16 show how vertical force and power vary as the flapping amplitude is increased for $f = 30$ Hz, $\tau_D = 0.36$, $\tau_U = 0.86$, and $\Delta\tau_R = 0.29$. Note that the stroke-plane angle varies as for Fig. 9. The translational velocity of the wing increases linearly with amplitude ϕ_0, which produces large changes in vertical force and power during the downstroke ($\tau = 0.0$–0.5). There is very little force produced on the upstroke ($\tau = 0.5$–1.0). The majority of the mean vertical force is produced by wing translation, with the rotations roughly canceling when time-averaged.

Figures 17 and 18 show the effect of varying the rotation rate. Here, $f = 30$ Hz, $\phi_0 = 34.5$ deg, and τ_D, τ_U, and $\Delta\tau_R$ were varied to keep the midpoint of the rotations constant at $\tau = 0.505$ and $\tau = 0.005$ (the same as for the varying-amplitude cases shown in Figs. 15 and 16). As the rotation rate is increased ($\Delta\tau_R$ decreased), the mean vertical force produced by the two rotations tends toward zero, whereas the mean power climbs rapidly.

This is reflected in Fig. 19, showing that the power economy drops rapidly as $\Delta\tau_R$ is decreased. The implication is that for stationary hover, a low rotation rate (high $\Delta\tau_R$) should be used to minimize power requirements. However, the large forces that can be generated by high wing rotation rates, as shown in Fig. 17, would be very useful for rapid maneuvering, at the expense of a large short-duration power input.

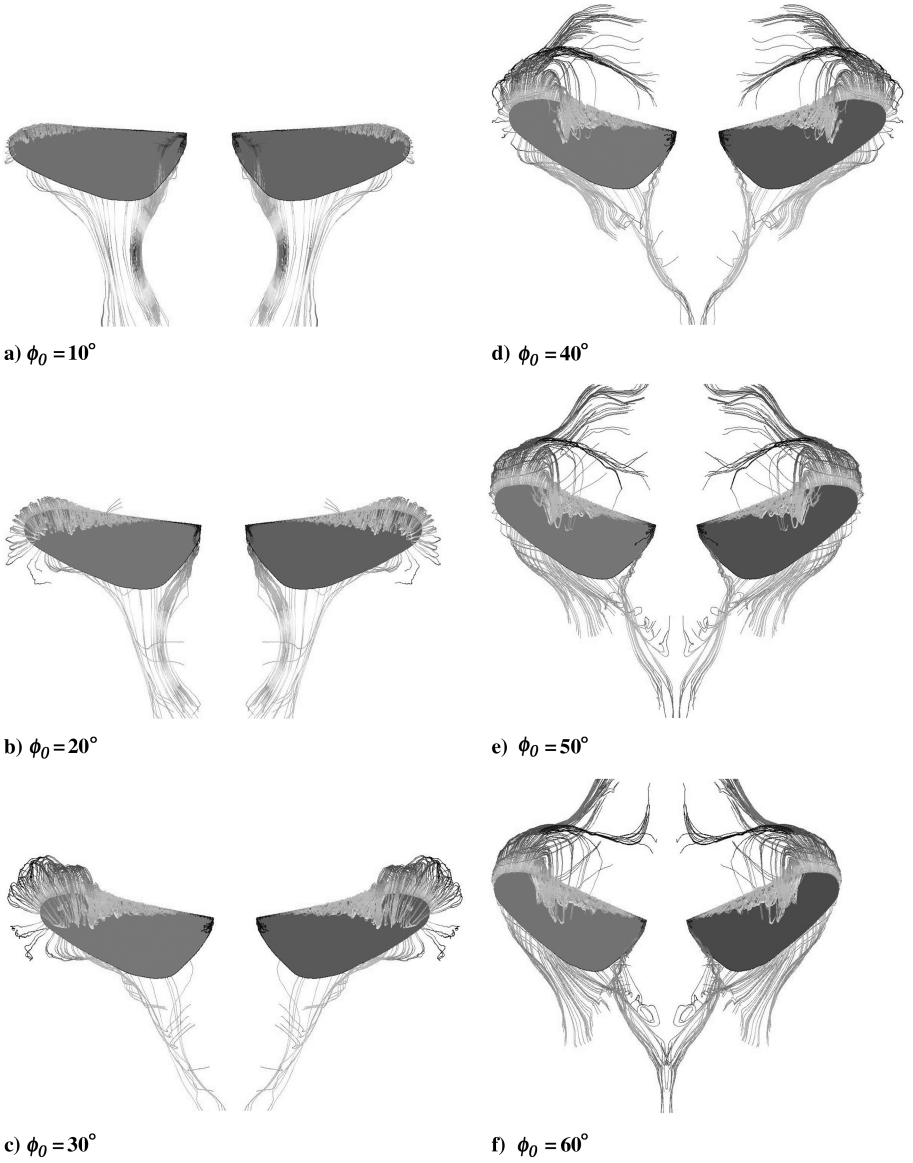

Fig. 14 Instantaneous streamlines for a range of flapping amplitudes ϕ_0, view from above, $f = 30$ Hz, wing moving downward at $t/T = 0.6$: a–c) the spiral leading-edge vortex remains attached to the wing for low amplitudes and d–f) the vortex bursts over the wingtips at high amplitudes.

IV. Conclusions

This work examined the effect of flapping amplitude, flapping frequency, and wing rotation timing and duration on the performance of a flapping wing in hover, based on the hind-wing shape and kinematics of a dragonfly, using a 3D Navier–Stokes computational solver. The coefficients of mean vertical force produced and power coefficients are shown to be essentially independent of frequency for $f > 5$ Hz, consistent with results reported in the literature. The power economy (ratio of mean vertical force produced to mean power required) shows a peak at a flapping amplitude of approximately $\phi_0 = 34.5$ deg for all the frequencies considered, which is also the amplitude reported in the literature for the dragonfly

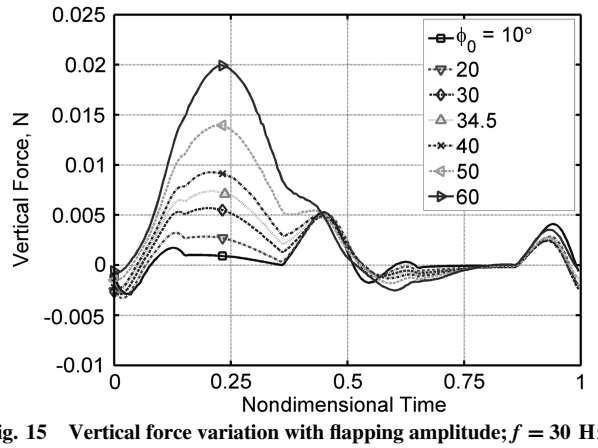

Fig. 15 Vertical force variation with flapping amplitude; $f = 30$ Hz.

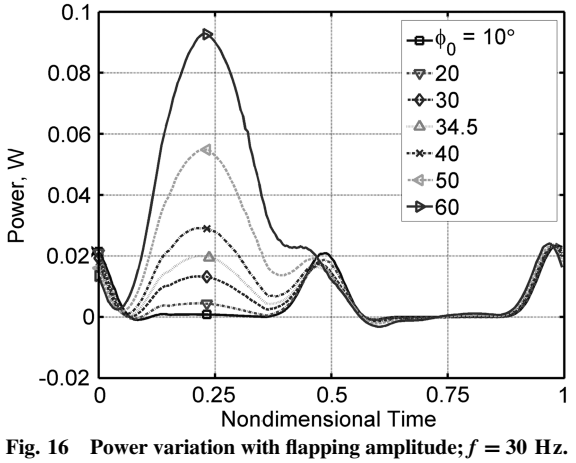

Fig. 16 Power variation with flapping amplitude; $f = 30$ Hz.

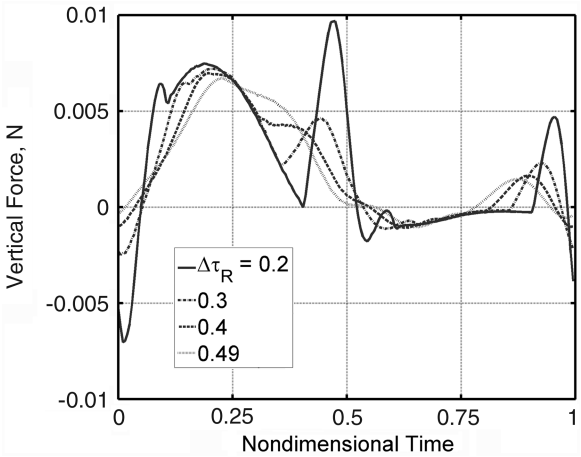

Fig. 17 Vertical force variation with rotation duration; $f = 30$ Hz and $\phi_0 = 34.5$ deg.

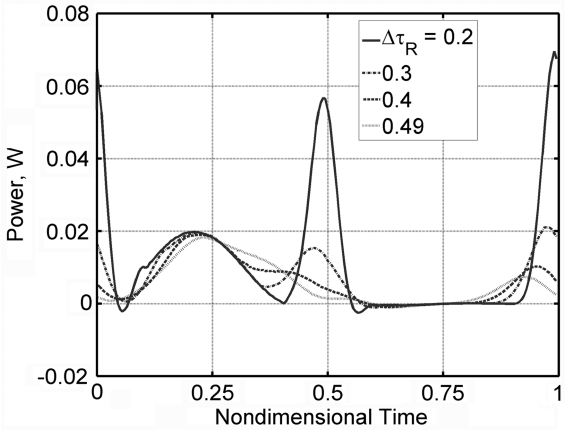

Fig. 18 Power variation with rotation duration; $f = 30$ Hz and $\phi_0 = 34.5$ deg.

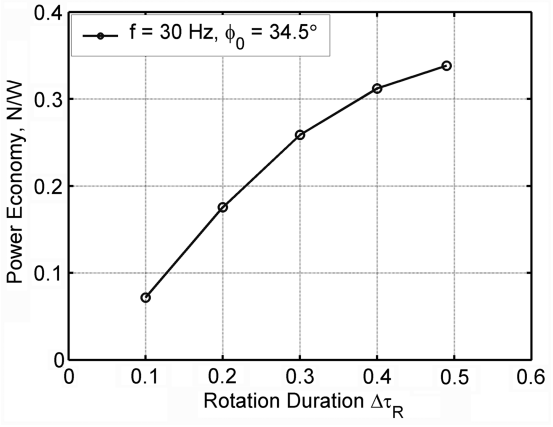

Fig. 19 Power-economy variation with rotation rate.

Aeschna juncea. Further work is required to determine the aerodynamic phenomena responsible for this peak and whether it holds for different wing planforms, more general kinematics, with wing flexibility accounted for, and with the effect of laminar to turbulent transition and a more accurate leading-edge geometry, potentially allowing for some modification of the precise flow separation point over the leading edge.

Acknowledgment

This work was supported by an award under the Merit Allocation Scheme on the National Facility of the Australian Partnership for Advanced Computing (APAC-NF).

References

[1] Ellington, C. P., "The Novel Aerodynamics of Insect Flight: Application to Micro-Air Vehicles," *Journal of Experimental Biology*, Vol. 202, No. 23, 1999, pp. 3439–3448; also available online at http://jeb.biologists.org/cgi/content/abstract/202/23/3439.

[2] Mueller, T. J. (ed.), *Fixed and Flapping Wing Aerodynamics for Micro Air Vehicle Applications*, AIAA, Reston, VA, 2000.

[3] Wang, Z. J., "Dissecting Insect Flight," *Annual Review of Fluid Mechanics*, Vol. 37, 2005, pp. 183–210. doi:10.1146/annurev.fluid.36.050802.121940

[4] Weis-Fogh, T., "Quick Estimates of Flight Fitness in Hovering Animals, Including Novel Mechanisms for Lift Production," *Journal of Experimental Biology*, Vol. 59, No. 1, 1973, pp. 169–230; also available online at http://jeb.biologists.org/cgi/content/abstract/59/1/169.

[5] Dickinson, M. H., Lehmann, F.-O., and Sane, S. P., "Wing Rotation and the Aerodynamic Basis of Insect Flight," *Science*, Vol. 284, No. 5422, 1999, pp. 1954–1960. doi:10.1126/science.284.5422.1954

[6] Dickinson, M. H., "Solving the Mystery of Insect Flight," *Scientific American*, June 2001, pp. 35–41; also available online at http://www.sciam.com/article.cfm?id=solving-the-mystery-of--i.

[7] Altshuler, D. L., Dickson, W. B., Vance, J. T., Roberts, S. P., and Dickinson, M. H., "Short-Amplitude High-Frequency Wing Strokes Determine the Aerodynamics of Honeybee Flight," *Proceedings of the National Academy of Sciences of the United States of America*, Vol. 102, No. 50, 2005, pp. 18213–18218. doi:10.1073/pnas.0506590102

[8] Liu, H., Ellington, C. P., Kawachi, K., van den Berg, C., and Willmott, A. P., "A Computational Fluid Dynamic Study of Hawkmoth Hovering," *Journal of Experimental Biology*, Vol. 201, No. 4, 1998, pp. 461–477; also available online at http://jeb.biologists.org/cgi/content/abstract/201/4/461.

[9] Sane, S. P., and Dickinson, M. H., "The Control of Flight Force by a Flapping Wing: Lift and Drag Production," *Journal of Experimental Biology*, Vol. 204, No. 15, 2001, pp. 2607–2626; also available online at http://jeb.biologists.org/cgi/content/abstract/204/15/2607.

[10] Norberg, R. A., "Hovering Flight of the Dragonfly *Aeschna Juncea L.*, Kinematics and Aerodynamics", *Symposium on Swimming and Flying in Nature*, Vol. 2, California Inst. of Technology, Pasadena, CA, 1974, pp. 763–781.

[11] Wakeling, J. M., and Ellington, C. P., "Dragonfly Flight, Part 2: Velocities, Accelerations and Kinematics of Flapping Flight," *Journal of Experimental Biology*, Vol. 200, No. 3, 1997, pp. 557–582; also available online at http://jeb.biologists.org/cgi/content/abstract/200/3/557.

[12] Wang, Z. J., "The Role of Drag in Insect Hovering," *Journal of Experimental Biology*, Vol. 207, No. 23, 2004, pp. 4147–4155. doi:10.1242/jeb.01239

[13] Sun, M., and Lan, S. L., "A Computational Study of the Aerodynamic Forces and Power Requirements of Dragonfly (Aeschna Juncea) Hovering," *Journal of Experimental Biology*, Vol. 207, No. 11, 2004, pp. 1887–1901. doi:10.1242/jeb.00969

[14] Yamamoto, M., and Isogai, K., "Measurement of Unsteady Fluid Dynamic Forces for a Mechanical Dragonfly Model," *AIAA Journal*, Vol. 43, No. 12, 2005, pp. 2475–2480.

[15] Norberg, R. A., "The Pterostigma of Insect Wings and Inertial Regulator of Wing Pitch," *Journal of Comparative Physiology*, Vol. 81, No. 1, 1972, pp. 9–22. doi:10.1007/BF00693547

[16] Huang, H., and Sun, M., "Dragonfly Forewing-hind wing Interaction at Various Flight Speeds and Wing Phasing," *AIAA Journal*, Vol. 45, No. 2, 2007, pp. 508–511. doi:10.2514/1.24666

[17] Usherwood, J. R., and Ellington, C. P., "The Aerodynamics of Revolving Wings, 1: Model Hawkmoth Wings," *Journal of Experimental Biology*, Vol. 205, No. 11, 2002, pp. 1547–1564; available online at http://jeb.biologists.org/cgi/content/abstract/205/11/1547.

[18] Wu, J. H., and Sun, M., "Unsteady Aerodynamic Forces of a Flapping Wing," *Journal of Experimental Biology*, Vol. 207, No. 7, 2004, pp. 1137–1150. doi:10.1242/jeb.00868

[19] Vogel, S., *Life in Moving Fluids: The Physical Biology of Flow*, Princeton Univ. Press, Princeton, NJ, 1994.

X. Zhong
Associate Editor